Multiple representative interactive linear eddy model: Investigation of turbulence chemistry interaction and evaluation of progress variable

(article starts on next page)

Full length article

Multiple representative interactive linear eddy model: Investigation of turbulence chemistry interaction and evaluation of progress variable definition and PDFs

Nidal Doubiani [a,*], Michael Oevermann [a,b]

[a] *Chalmers University of Technology, Gothenburg, Sweden*
[b] *Brandenburgische Technische Universität Cottbus-Senftenberg (BTU), Cottbus, Germany*

ARTICLE INFO

ABSTRACT

Improving the predictions of unsteady effects in combustion processes requires novel combustion models that include turbulence chemistry interaction effects. The Multiple Representative Interactive Linear Eddy Model (MRILEM) is an improved version of the previous RILEM variant. MRILEM utilizes a pressure coupling instead of a volume constraint to intrinsically include heat effects into the LEM line with no supplementary modeling. In addition, it advances multiple LEM lines in parallel to improve statistical fidelity. The pressure coupling of MRILEM generates a coupling effect between the LEM lines that assists in communicating the combustion process between the lines. The "Spray-B" engine of the Engine Combustion Network (ECN) was simulated using MRILEM. While the original RILEM variation employs a straightforward Dirac δ-peak for the progress variable, a realistic PDF requires this function to extend over the entire space. The introduced MRILEM compares the utilization of two progress variable PDFs, namely a step function defined based on the mean and a β-PDF generated from the progress variable mean and variance. The progress variable variance was calculated based on the Pierce and Moin formulation with a RANS adaptation based on the integral length scale. In addition, two definitions of the progress variable are investigated, namely O_2 and h_{298}. A tabulation method is introduced for RILEM to reduce the computational time by advancing pre-generated LEM solution matrices constructed in mixture fraction Z and progress variable c spaces. The different variants of the model, i.e., MRILEM-β_Z-Step$_c$, MRILEM-β_Z-β_c, TRILEM-β_Z-Step$_c$, and TRILEM-β_Z-β_c were compared against experiments based on heat release rate, ignition delay, flame lift-off, and computational time.

1. Introduction

Both the need for transportation of goods in local and global markets as well as the human desire to travel are met by a huge and increasing transportation sector. Internal combustion engines remain the dominant energy source in the global transport sector. According to the 2050 Net Zero Emissions scenario, ICEs are projected to power 80% of the car and van fleet by 2030 [1]. However, fossil fuel combustion produces harmful emissions that threaten human health and environmental sustainability. E.g., carbon monoxide (CO) causes more than half of the worldwide fatal poisoning cases [2], nitrogen monoxide (NO) is quite harmful to the respiratory system and increases the general acidity level of the environment [3]. In addition, particulate matter (PM) generated from operating vehicles can lead to lung cancer, DNA damage, and premature death [4]. Decreasing these emissions is directly linked to improving the combustion process in internal

combustion engines, utilizing alternative fuels and/or advanced exhaust after-treatment systems (EATS). Several measures were taken worldwide to enhance air quality by introducing stringent legislation such as China VII or Euro VII that enforce a progressive decrease in the number of pollutants and their concentrations [5] from combustion processes. Although sophisticated EATS system can satisfy some of the introduced standards, its price and complexity will substantially increase, making it less and less attractive for both the producer and the consumer. Therefore, almost all OEMs (Original Equipment Manufacturer) continuously shift from ICE to Hybrid-Electric, Battery-Electric (BEV) and Fuel-Cell (FC) powered vehicles. Although BEVs can and will help to substantially improve air quality – in particular in urban areas – their carbon footprint depends on clean electricity production such as wind and solar [6]. A similar narrative is applied to FC vehicles. Although it has a promising potential in reducing harmful emissions

compared to conventional fossil-fuel powered vehicles [7], hydrogen-powered vehicles, either ICE or FC, carry a significant risk, namely the possibility of explosions due to leaks from the hydrogen tank [8]. Although the transition from a combustion driven to an electricity based transportation system seems realistic for light and medium duty vehicles in the foreseeable future, it is quite likely to see combustion driven powertrains for systems with very high energy demand such as long distance trucks, ships and aircrafts for many decades to come. Therefore, there is still a demand for research and development activities to further improve combustion systems in order to minimize the impact of such combustion driven systems on global warming and air quality.

An integral part of any product development and optimization cycle are detailed numerical simulations of the relevant physical processes. In terms of optimizing combustion engines, CFD investigations combined with turbulence and combustion models are utilized to optimize the combustion process inside the ICE. Although engine combustion simulations are routinely done, there is still room and need for improving the predictive capabilities of turbulent combustion models, in particular with respect to pollutant formation which is heavily influenced by the strongly non-linear interaction of turbulence and chemistry. Well established and heavily used turbulent combustion models in engine research include perfectly stirred reactor (PSR) models [9–11], partially stirred reactor models (PaSR) [12–14], flamelet models for non-premixed [15,16] and premixed combustion [17,18], flamelet generated manifold methods [19,20], conditional moment closure models [21,22] and so-called transported Probability Density Function (PDF) models [23,24].

Many of the cited combustion models are designed for either pre-mixed or non-premixed combustion. Often, they also assume chemical time scales to be much shorter than turbulent time scales which allows for a parametric description of turbulence-chemistry interactions as in flamelet models or the partially stirred reactor (PaSR) model. However, advanced combustion concepts for low emission and high efficiency combustion such as partially premixed combustion operate under conditions where standard combustion models are (in principle) not valid and their predictive capabilities might be limited.

In this article, combustion closure is achieved utilizing the linear eddy model (LEM) [25–27] in a representative way. LEM time-advances all relevant scalar properties such as species mass fractions and temperature on a one-dimensional line resolving all scales under the assumption of a prescribed turbulence spectrum. Turbulent eddies are represented via stochastic mapping events. LEM is one of the few combustion closure models which can be regarded as fully mode and regime independent. It was used in many studies as a stand-alone model, showing its capability to capture turbulence chemistry interaction effects [28]. Moreover, LEM was utilized to assess the impact of varying turbulent length scales on the construction of single-point PDFs for isentropic, homogeneous stationary turbulence [29]. It was also used to investigate molecular diffusion effects by varying Reynolds and Schmidt numbers [30] , and to predict intermediate species such as CO [31].

In LES-LEM an LEM is solved in each cell of a large-eddy simulation [32–36]. It has been successfully applied for both premixed [37], non-premixed [38] and partially premixed combustion simulations [39].

The LES-LEM approach was recently extended to an approach called super-grid LES-LEM [40], where instead of advancing an LEM line in each LES cell, the LEM lives in a (larger) cluster of LES cells. This technique was assessed against DNS data for a premixed backward-facing step case in [41], where primary and intermediate species, such as CO_2 and OH, and their reaction rates were assessed. It also showed a substantial decrease in the computational time compared to traditional LES-LEM. However, computational demands for LES-LEM and supergrid LES-LEM are high, making the approach less suitable for practical or industrial applications.

LEM was likewise coupled to RANS simulations for round jet cases in its planar form in [42] and in a LEM3D form in [43], where the combustion closure was achieved on three orthogonal LEM lines to capture potential 3D effects while reducing the computational time. A spherical formulation suitable for ICE applications called RILEM was presented in [44]. In the original version of RILEM, a single LEM line is used to represent the complete combustion chamber. Coupling to the RANS CFD simulation was achieved as in flamelet models with a presumed PDF approach for the mixture fraction only. RILEM was tested for a constant volume combustion chamber in [44] and compared against a multiple representative interactive flamelet model (mRIF) in [45]. An advanced formulation of RILEM based on mixture fraction and progress variable was introduced in [46] for a heavy-duty engine case. In [44–46], coupling between LEM and CFD domains was based on a volume constraint, which conveys that heat effects were modeled separately on the LEM line to maintain the representative aspect between the CFD and the LEM. A new RILEM variant based on a pressure coupling was introduced in [47].

This paper utilizes RILEM to simulate the combustion process for a moving piston case in two variants, i.e., Multiple RILEM (MRILEM) and Tabulated RILEM (TRILEM). The reason behind utilizing MRILEM is to increase the statistical fidelity of the LEM solution by advancing the same turbulence parameters, i.e., $\tilde{k}$ and $\tilde{\varepsilon}$ on parallel LEM lines but with different eddy placements. The effect of advancing multiple lines compared to a unique line was highlighted in [47]. However, in this article, as explained later, the LEM solution is not initialized empty as in the previous study. Instead, a prebuilt 0D reactor solution is used. TRILEM, on the other hand, is a tabulated technique to reduce computational time by only advancing the CFD solver and gathering the scalar statistics from a prebuilt LEM solution table.

Although turbulence chemistry interaction (TCI) in RILEM is mainly captured on the LEM line, the coupling with the CFD using a presumed PDF introduces an additional aspect of TCI. To evaluate the impact of the chosen presumed PDF, we simulate two different PDF shapes for progress variable: a step-function PDF and the well-known β-PDF. Furthermore, two different definitions of the reaction progress variable, oxygen and formation enthalpy, are investigated. Results are compared to experiments.

This article is organized as follows: This introduction is followed by a thorough description of the mathematical model in the second section. The study's numerical and experimental setup are explained in the third section, and the findings are presented and discussed in the fourth section. Finally, a conclusion summarizing the most relevant findings of the work is given.

2. Mathematical model

2.1. Linear Eddy model

LEM was first suggested by Kerstein [25,26] as a turbulent scalar mixing model for non-reactive flows and was then extended to include reactive flows [48,49]. LEM is based on advancing molecular diffusion and turbulence advection as two independent concurrent processes. Molecular diffusion is advanced on the one-dimensional LEM line by solving 1-D balance equations for species mass, energy and an equation of state. The LEM transport equations are advanced using a second-order scheme that uses a standard central discretization of the diffusion terms. In the case of reacting flows, the LEM transport equations of species and energy will incorporate stiff chemical source terms that need to be integrated, which here is realized with SUNDIAL's BDF method [50]. In addition, transport and thermophysical properties are assessed using the CANTERA package [51]. Turbulent advection on a 1D line is realized by triplet map processes that mimic the effect of the 3D vortices. The LEM eddies require three key parameters:
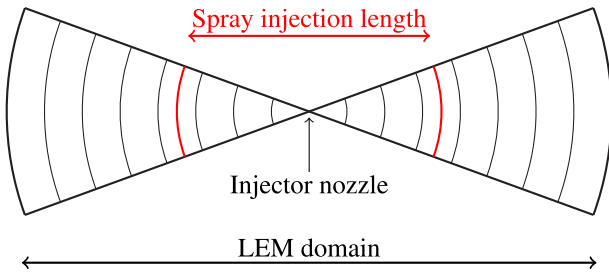
Fig. 1. Representation of the spray on the spherical double-coned LEM.

Fig. 2. Pressure coupling RILEM code framework.

- Eddy size: Based on a size distribution defined based on the turbulence subrange between the integrated and Kolmogorov length scales.
- Eddy position: Uniformaly sampled on the line in case of homogeneous turbulence.
- Eddy event realization: Based on a Poisson process sampling that utilized the mean occurrence time.

In addition to turbulent eddies representing stochastic (isotropic) turbulence, LEM has recently been extended to model large-scale motions such as swirl and tumble, which are relevant in combustion chambers of engines [52]. This has been achieved with an identical mapping procedure as for small-scale turbulent eddies but with an important distinction: The eddy size of the large-scale eddies is fixed to half of the combustion chamber bore. Large scale eddy's position is uniformly sampled on the line with an eddy time-scale based on the spray velocity, which drives the large-scale motion in the engine considered here. The total number of large eddies is calculated at the start of the simulation based on the fuel injection duration, spray velocity, and domain length. This is not the case for the small-scale turbulent eddies in LEM as they are modeled based on the integral and Kolmogorov scales of turbulence, which are deduced at runtime from the turbulence model on the CFD side. Although LEM describes the statistical state along a (representative) one-dimensional line of sight through a given physical space (here: the combustion chamber), the line can represent different geometries: planar, cylindrical, or spherical. In this work, which handles reactive spray simulation inside of an engine, LEM was chosen to be utilized in its spherical formulation, which is based on two solid cones that are oriented in the direction of the spray axis, see Fig. 1. This choice is motivated by consideration to capture volumetric effects on a one-dimensional line, e.g., to match global equivalence ratio and characteristic mixing length scales on the LEM with the 3D CFD, see [53] for a detailed discussion.

2.2. RILEM coupling

As presented before in [47,53], RILEM is based on coupling one or several LEM lines representing fuel-air mixing and combustion with a CFD solver. In its latest development stage, coupling between CFD and LEM is on one side achieved via pressure, i.e. the thermodynamic pressure of the CFD domain is enforced on the LEM line, which allows for a consideration of heat loss effects due to wall heat losses and latent heat of evaporation, represented via detailed models on the CFD side, on the LEM domain without explicit modeling of those effects on the LEM line. In addition, the CFD solver provides in each time step of the simulations the evaporated fuel mass the spray vapor penetration length and LEM driving turbulence parameters to the LEM. After advancing the LEM solution for the given time step, LEM scalar solution values are conditioned to mixture fraction and progress variable space and averaged with a presumed PDF. As a result, the LEM provides mean values for species mass fractions and the mean reaction progress variable source term to the CFD solver, see Fig. 2 and the presentation below. The coupling technique requires a so called
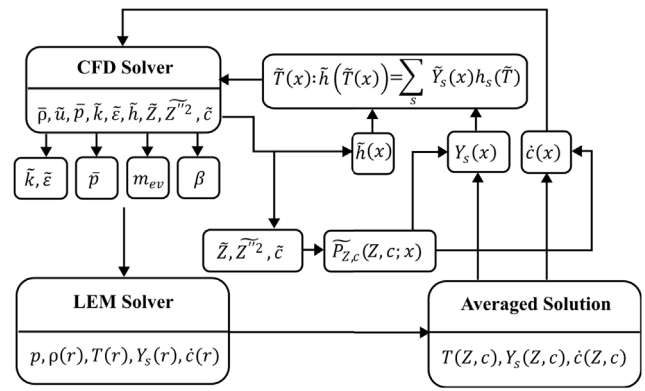
split operator strategy, which was explained thoroughly in [31,47]. The spherical formulation of LEM requires specific adaptations, namely the form of LEM transport equations and triplet maps as described in [53,54]. A detailed documentation of the LEM model formulation as used in study has recently been given in [47] and will not be repeated here for brevity.

The 3D governing equations for global mass, momentum, and energy are advanced with a RANS turbulence model. In models such as PSR or PaSR, transport equations for all species are advanced on the CFD domain. RILEM is based on a similar approach as RIF [55] and advanced transport equations for mean and variance of mixture fraction Z and mean of progress variable c, see [47] for details.

On the LEM side, the mixture fraction is defined based on Bilger's formulation [56], and the combustion progress variable is defined as

$$c = \frac{\psi - \psi_u}{\psi_b - \psi_u}, \qquad (1)$$

where subscripts u and b, respectively, represent the unburnt and burnt values of a chosen reactive scalar. In case ψ is calculated based on a chemical species, the progress variable source term $\dot{c}$ is evaluated in each LEM cell via

$$\dot{c}(Z,c) = \frac{1}{\psi_b - \psi_u} \frac{d\psi}{dt}, \qquad (2)$$

with

$$\frac{d\psi}{dt} = \frac{\mathcal{R}_\psi W_\psi}{\rho}, \qquad (3)$$

where $\mathcal{R}_\psi$ denotes the reaction rate of volume specific scalar ψ, W_ψ is the molecular weight of scalar ψ. It is important to note that ψ can represent a combination of representative reactive scalars. In this article, two different definitions of ψ are considered: In the first case, ψ is equal to the oxygen mass fraction Y_{O_2}, in the second case, ψ represents the specific enthalpy at standard conditions h_{298}.

If ψ is based on h_{298}, the subscripts u and b will represent the formation enthalpy based on the unburnt and burnt species, respectively. $\frac{dh_{298}}{dt}$ is calculated as follows :

$$\frac{dh_{298}}{dt} = \frac{\sum_s h_{298,s} \mathcal{R}_s W_s}{\rho}, \qquad (4)$$

As written above, feedback from the LEM to the CFD solver is realized by a mapping procedure that starts with conditioning the scalar values ϕ on mixture fraction and progress variable space. The reactive scalars ϕ are integrated on the CFD side based on the following:

$$\tilde{\phi} = \int_0^1 \int_0^1 \phi(Z,c) \, \widetilde{P}_{Z,c}(Z,c) \, dZ \, dc, \qquad (5)$$

where $\widetilde{P}_{Z,c}(Z,c)$ denotes the joint probability density function of Z and c. The statistical independence assumption allows the simplifications of
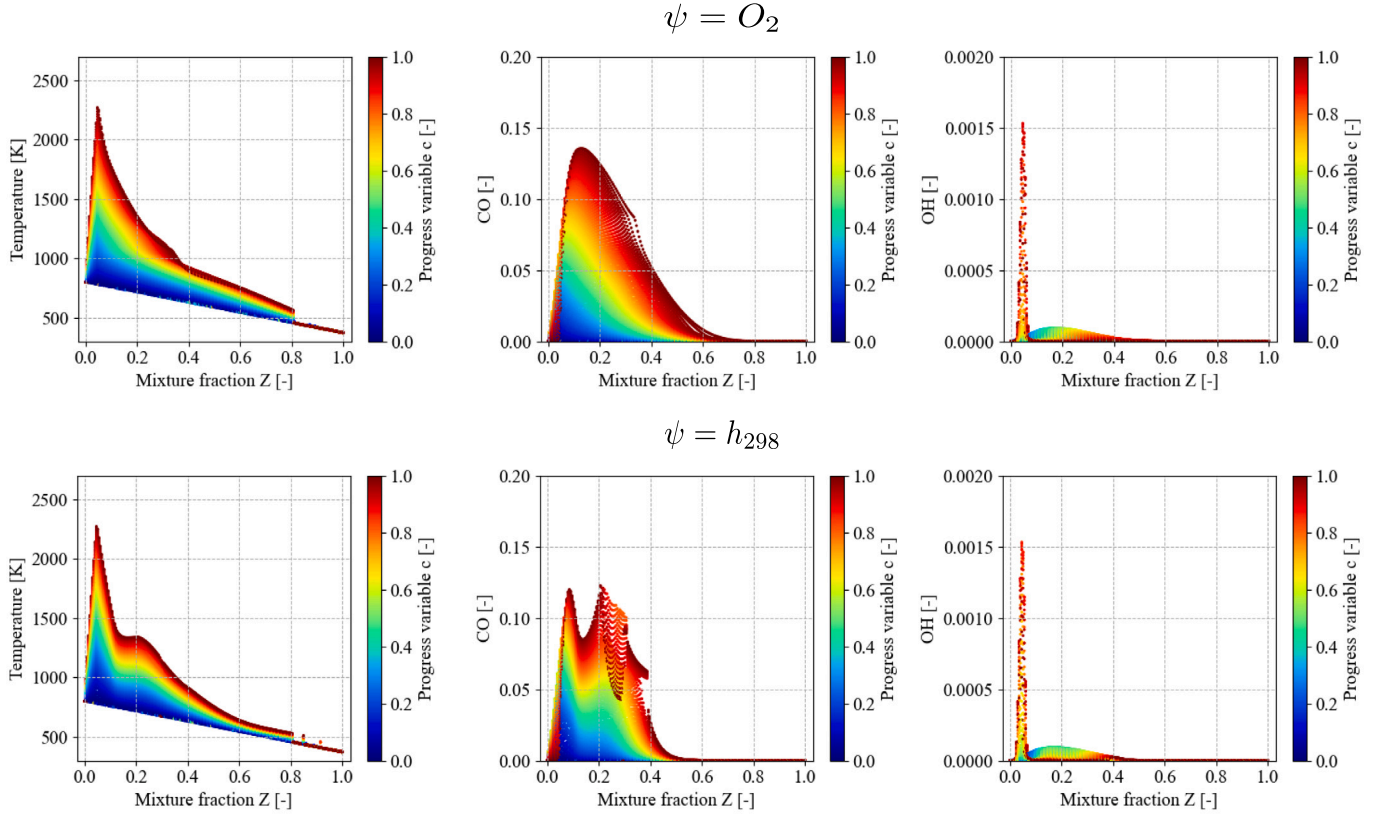
$$\psi = O_2$$

$$\psi = h_{298}$$

Fig. 3. Scatter plots of the 0D reactor solution in mixture fraction space for $\psi = O_2$ (above) and $\psi = h_{298}$. (below). The reactive scalars are temperature, CO mass fraction, and OH mass fraction at ambient temperatures at top dead center (TDC) T = 900 K.

the joint PDF to a multiplication: $\tilde{P}_{Z,c}(Z,c) = \widetilde{P}_Z(Z)\,\widetilde{P}_c(c)$, which makes the integration as follows:

$$\tilde{\phi} = \int_0^1 \int_0^1 \phi(Z,c)\,\widetilde{P}_Z(Z)\,\widetilde{P}_c(c)\,dZ\,dc. \tag{6}$$

The transport equations of $\tilde{Z}$, $\widetilde{Z''^2}$ and $\tilde{c}$ previously presented in [47] are advanced on the CFD side. Quantifying $\tilde{Z}$, $\widetilde{Z''^2}$ locally enables the construction of a unique shape of the presumed β-PDF in each cell of the computational grid for Z, which is the same approach utilized in RIF. In [46], integration in the progress variable space was achieved using a Dirac δ peak in case the solution table is complete in c space. Since the investigation in this work does not guarantee the completion of the solution table, the step PDF defined uniquely on the progress variable mean, previously introduced in [47] was utilized combined with a solution history persistence to avoid the empty slots issue. The step PDF is defined as the following:

$$\tilde{P}_c(c;\tilde{c}) = \begin{cases} \frac{1-\tilde{c}}{\tilde{c}} & 0 \le c < \tilde{c}, \\ \frac{\tilde{c}}{1-\tilde{c}} & \tilde{c} \le c \le 1. \end{cases} \tag{7}$$

The reason behind utilizing a step function was twofold: (i) The inclusion of the development of the reactive scalar on the totality of the progress variable space. (ii) Scaling the PDF because of empty slots in the solution table requires a function defined on the entirety of the progress variable space, contrary to a Dirac δ peak. In this work, the step function PDF and the β-PDF are tested for integration in progress variable space.

3. RILEM solution initialization

To avoid scaling of the PDF of Z and c, the reactive scalars solution tables are initialized as follows: First, the solution tables are initialized with an unburnt composition for all values of Z. Second, a collection

of 200 independent closed homogeneous reactors with compositions varying linearly from $Z = 0$ to $Z = 1$ are advanced. The unsteady homogeneous reactors were given enough time to ignite, except for $Z > 0.8$, where only the unburnt stat was considered, as could be observed in Fig. 3. This does not cause a problem as $\tilde{Z}$ in the CFD does not reach 0.8. The persistence of the LEM solutions is also utilized in this work. It is important to note that this initialization step is realized for each case since the ambient temperatures at TDC and the initial pressures are different, which influences the solution in Z and c space. Fig. 3 shows solutions of the reactive scalars temperature, mass fractions of CO and OH in Z,c spaces for $c(Y_{O_2})$ and $c(Y_{h_{298}})$ at a TDC ambient temperature of $T = 900$ K. The solution was not initialized for $\dot{c}$, implying that the auto-ignition process originates only from the LEM.

Two different PDFs for the progress variable are tested in this work: (i) A step function PDF, defined uniquely on the mean value $\tilde{c}$, was presented in detail in [47]. (ii) A β-PDF constructed uniquely from $\tilde{c}$ and $\widetilde{c''^2}$ similar to the mixture fraction. An algebraic model for the variance of the progress variable following [57] is utilized here:

$$\widetilde{c''^2} = C_\psi \Delta^2 |\nabla \tilde{c}^2|, \tag{8}$$

where C_ψ denotes a constant chosen as $\frac{1}{12}$. The variance model of [57] is suggested for LES simulations based on the filter width Δ. Since the current setup is for a RANS framework, the filter width is replaced with the integral length scale l_t, which is calculated as follows in each CFD cell:

$$l_t = \sqrt{\frac{3}{2}} \frac{c_\mu}{Sc_t} \frac{\tilde{k}^{3/2}}{\tilde{\varepsilon}}, \tag{9}$$

where $\tilde{k}$ and $\tilde{\varepsilon}$ denote the kinetic energy and the dissipation rate, respectively, as derived from the $k-\varepsilon$ model. The constant c_μ, set at 0.09, is taken from the standard $k-\varepsilon$ model. Additionally, Sc_t represents the Schmidt number, which is defined as 0.7.

4. Tabulated RILEM

4.1. LEM solution table

The Tabulated RILEM (TRILEM) methodology aims to enhance the computational efficiency of RILEM. This advancement is achieved by creating a solution table based on prior runs of multiple LEM lines. The tabulated solution can be constructed based on two primary strategies: (i) Conducting an initial CFD simulation using a conventional combustion model, e.g., WSR, to generate the required input parameters as outlined in [31]. These input parameters are then incorporated into multiple spherical stand-alone LEMs that are advanced to construct the solution table. (ii) Advancing MRILEM and storing the solution table at the end of the simulation. In this work, the latter method is utilized for building the TRILEM solution table, since it requires less time. The construction of the TRILEM solution table involves the conditioning of the turbulent reactive scalars, namely, temperature T, primary and secondary species mass fractions Y_s, and progress variable source term $\dot{c}$ on mixture fraction Z and progress variable c. Similar to RILEM, the governing equations of continuity, momentum, energy, mean mixture fraction $\tilde{Z}$, variance of mixture fraction $\widetilde{Z''^2}$ and mean of progress variable $\tilde{c}$ are advanced. The integration of the turbulent reactive scalars is realized in a manner similar to RILEM by employing P_Z and P_c. However, unlike RILEM, no LEM line is advanced in TRILEM. The quantification of the turbulent reactive scalars relies only on the PDFs of Z and c and the pre-constructed solution table. While TRILEM provides promising outcomes, as demonstrated in the results section, there are notable limitations. The process of building the table involves a spectrum of turbulence levels dictated by the CFD spray injection process. Consequently, the table contains information reflecting a range of turbulence histories within the combustion chamber. A more sophisticated table would be constructed by incorporating an additional parameter, such as turbulence diffusivity D_t or turbulent Reynolds number Re_t, to capture the local effect of turbulence on combustion in each computational cell in a more accurate way. This would also require a PDF to integrate the reactive scalars within that specific turbulence space D_t or Re_t. This aspect, however, is not explored in this investigation and would be the subject of future research.

5. Test case

The experimental case under investigation in this work is a standard test case for model validation, namely Spray-B from the Engine Combustion Network (ECN). It is a heavy-duty spray combustion case with n-dodecane as the fuel and a piston displacement volume of 2.34 l. The details of the case can be found in [58]. In this study, three cases are investigated, each identified by the Top Dead Center (TDC) ambient temperature, specified as T = 800 K, 900 K, 1000 K. For each of these cases, the in-cylinder conditions are characterized by an oxygen concentration that constitutes 15% of the total volume of the gas mixture in the cylinder, a density of $\rho = 22.8$ kg/m^3, and a fuel injection pressure of 1500 bar.

6. Numerical setup

The LEM simulations are performed with a code based on [54] which has been utilized in previous RILEM studies before [44,47]. The code was modified in [47] for RILEM pressure coupling. The simulation utilizes a chemical mechanism of 54 species and 256 chemical reactions proposed by [59]. The CFD simulations were realized using OpenFOAM version 2.2.x [60] combined with the libICE library for mesh generation [61] and spray modeling. Turbulence is taken into account with a RANS approach using the standard $k - \epsilon$ model, where the model constant $C_{\epsilon 1} = 1.54$ was adjusted as recommended by the ECN workshop for diesel combustion simulations [62]. A Lagrangian approach is used to represent the dispersed liquid spray. Fuel parcels

have been injected based on the blob injection model, which implies that the diameter of the initial parcels is equal to the diameter of the nozzle exit hole. Modeling secondary breakup was based on the KH-RT hybrid model combining two instability mechanisms of Kelvin–Helmholtz (KH) and Rayleigh–Taylor (RT). The KH instability manifests as a wave on the droplet surface. This wave continues to grow due to the aerodynamic forces induced by the difference between the velocity of the droplet and the surrounding gas. Once the growth rate of this wave reaches a maximum value, a child droplet is created. The RT instability, on the other hand, is due to the density difference of two interacting fluids in case of acceleration, where the interface is considered stable if the acceleration is oriented into the dense fluid. The outcome of RT instability is droplet disintegration into several child droplets with a diameter proportionate to the wavelength Λ of the parent droplet defined as $\Lambda = C 2\pi \sqrt{\frac{3\sigma}{a(\rho_l - \rho_g)}}$ where C represents an adaptable constant, σ the surface tension between two fluids, a the acceleration of the interface based on the drag coefficient C_D and the relative velocity of fluids u_{rel} and ρ_l and ρ_g are the densities of the liquid and the gas, respectively. Heat transfer between the liquid and gaseous phase was modeled with the well-known Ranz–Marshall correlation [63].

7. Results and discussions

We present results for two different flavors of RILEM: MRILEM and TRILEM. Each approach was advanced for two different progress variable definitions, one based on O_2 mass-fraction and one on h_{298}, and two different assumed PDFs for the progress variable, namely step function PDF and β-PDF.

7.1. Multiple RILEM with 0D reactor initialization

The MRILEM simulations were initialized using a species solution table derived from a 0D homogeneous reactor solution, as partially illustrated in Fig. 3. This initialization strategy serves two primary purposes. First, it allows the investigation of the effect of MRILEM initialization with a solution that incorporates a meaningful distribution of species both in Z and c instead of an empty solution as in [47], an unburnt, or a solution based on linearly interpolated mass fractions. However, the 0D homogeneous reactor initial solution does not account for molecular diffusion, heat conduction, and turbulence advection. The second reason is to minimize the effect of the PDF scaling technique, particularly at the start of the simulation as this technique can lead to an over-representation of the statistics uncovered by stochastic eddy events.

7.1.1. Analysis of LEM and 0D solution in (Z, c) space

Fig. 4 provides a more detailed presentation of some 0D reactor solutions displayed in 3, where particular bins of Z and c were selected to be depicted in both Z, c space. Fig. 4 essentially encapsulates the evolution of the 0D reactor solution table after introducing molecular diffusion and heat conduction alongside turbulence via multiple LEMs. A first observation is the difference in the 0D reactor solution distribution for $c(Y_{O_2})$ and $c(h_{298})$, which can be observed in the shape of temperature and CO in Z space, namely the drop at $Z \approx 0.14$. In addition, the peak value of CO in c space is also different between $c(Y_{O_2})$ and $c(h_{298})$, where it peaks in $Z \approx 0.65$ in $c(Y_{O_2})$; meanwhile, it peaks $Z \approx 0.58$ for $c(h_{298})$. The last point would be OH distribution in Z space, where it reaches a lower value at $c = 1$ for $c(h_{298})$ than in $c(Y_{O_2})$. In addition to the 0D reactor solution, this figure compares the solution initialized with the 0D reactor and the solution assembled from the LEM lines advancement for specific Z and c bins, featuring diffusion and turbulent mixing. In progress variable space, the LEM solution yields a lower value than the 0D reactor for both $c(Y_{O_2})$ and $c(h_{298})$. This is due to heat conduction towards colder cells in the surroundings, which
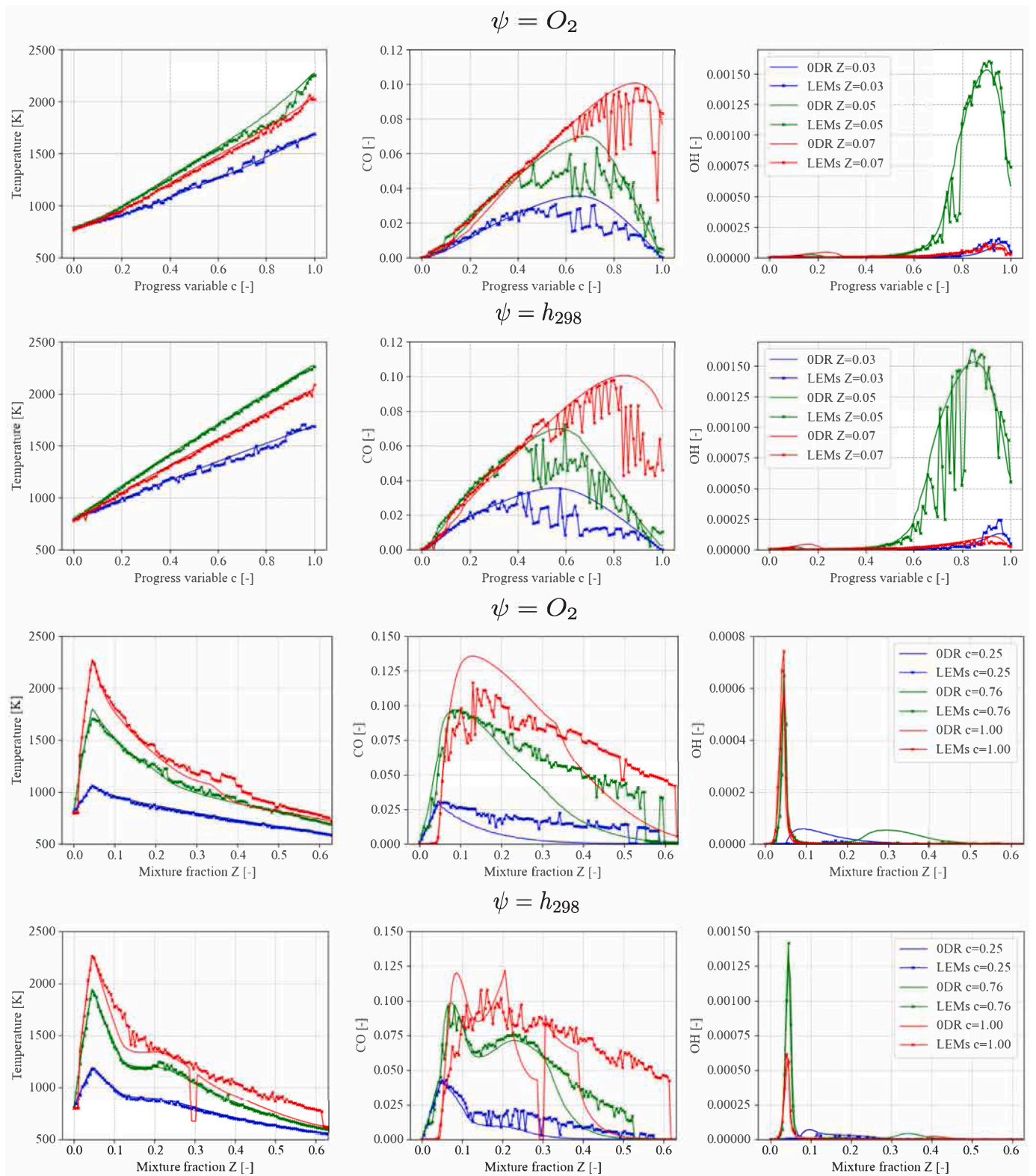
Fig. 4. Comparison of statistics of reactive scalars T, CO and OH, generated from the 0D reactor and the LEM advancement in progress variable space (above) and mixture fraction space (below) for both $\psi = O_2$ and $\psi = h_{298}$. at $T = 900$ K.
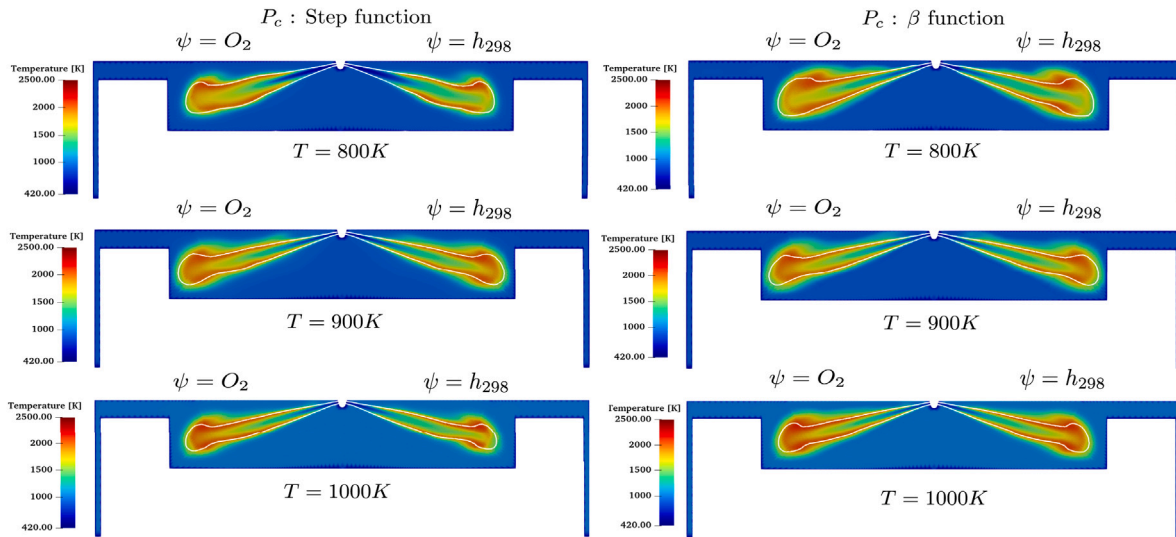
Fig. 5. CFD representation of instantaneous temperature profiles at CAD = 364, where the white iso-contour represents Z_{st}.
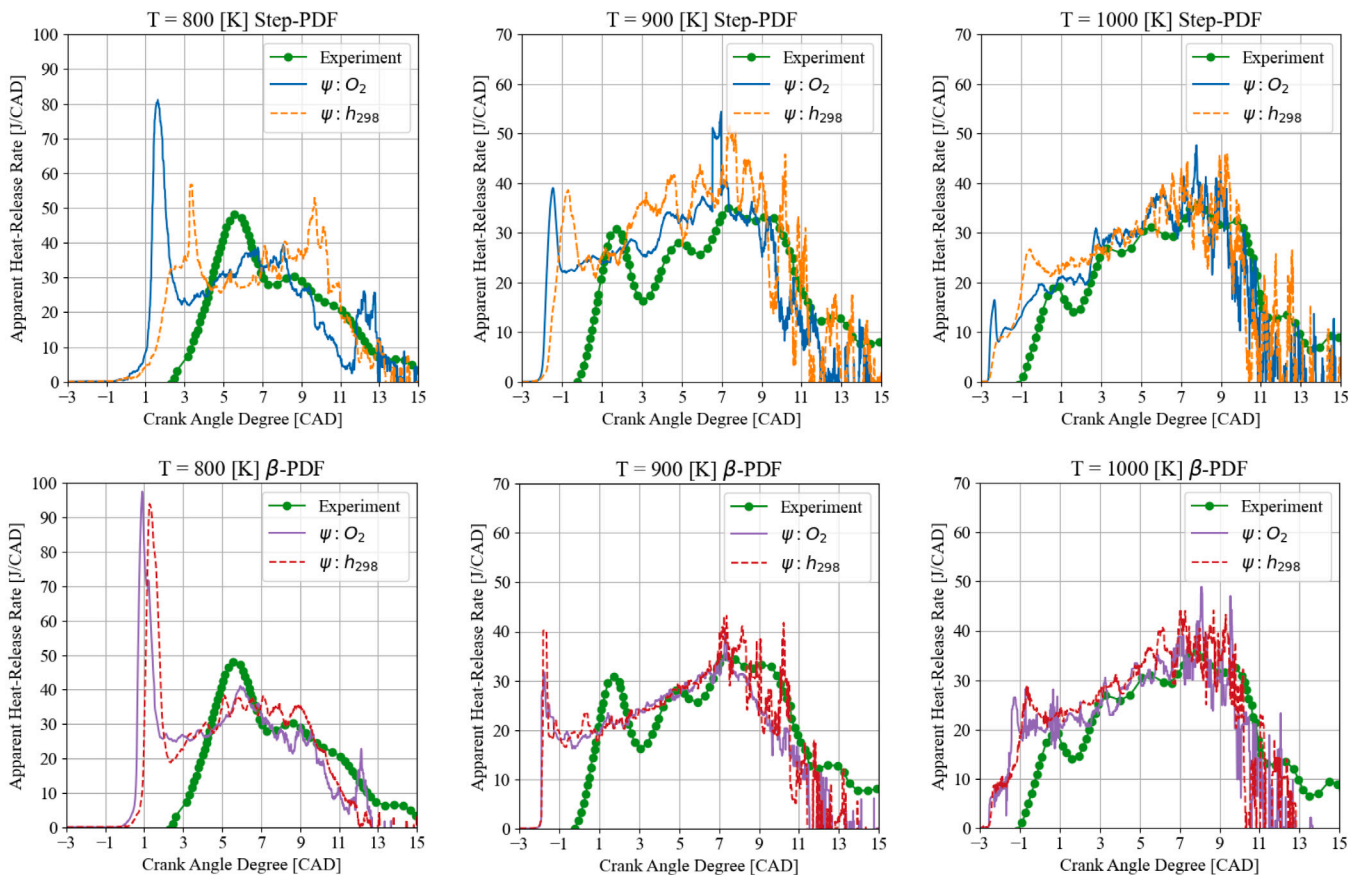

Fig. 6. Comparison of heat release rates for MRILEM for $\psi = O_2$ and $\psi = h_{298}$, and P_c: step (above) and P_c: β (below) with experiments at $T = 800$ K, 900 K and 1000 K.

influences the solution due to turbulence and diffusion in physical space. Investigating the solutions in c space shows that the trend of the LEM solutions follows the same trend as the 0D reactor solutions. However, when examining the solution on Z space, it appears that the statistics uncovered from the LEM line differ from the 0D reactor solutions. This difference is well displayed in the CO distribution in Z space, where the solution spreads across Z space instead of maintaining the initial form of the 0D reactor. For c(Y_{O_2}), the peak at $Z \approx 0.13$ seems

to have attenuated, and the lower values at $Z > 0.35$ have increased. This trend is the same for all the selected c bins. The spreading of the LEM solution can also be observed for OH mass fraction in Z space, where the high values at $Z \approx 0.1$ and $Z \approx 0.3$ have been attenuated. Similar behavior is observed for c(h_{298}); however, the drop at $Z \approx 0.14$ seems to be respected even by the LEM solution; this is well observed for bin $c = 0.76$. In addition, the drop can also be observed when comparing the temperature profiles. The conclusion would be that the
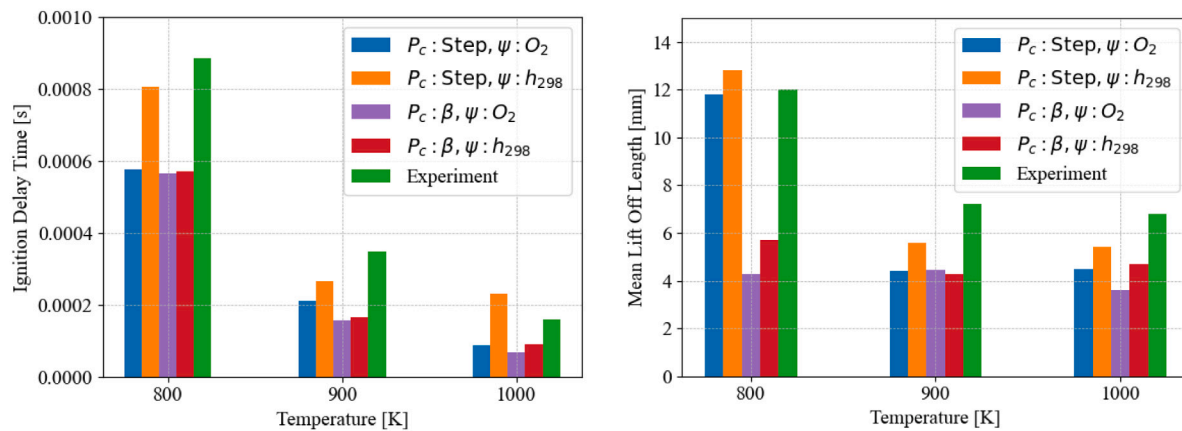
Fig. 7. Comparison of MRILEM ignition delay time (left) and Flame lift-off length (right) with experiments.

effect of altering the progress variable definition is not overwritten by the turbulence chemistry interaction presented by LEM, at least not for these two definitions. The comparative analysis of LEM and 0D reactor solution shows effects that are attributed to both diffusion and turbulence, which are not present in the homogeneous reactor simulations. Comparing statistics derived from unsteady flamelet simulations with LEM statistics would also be of interest since both encapsulate the impact of molecular diffusion and heat conduction, thus isolating the difference to be solely from the turbulence chemistry interaction. However, this analysis could be explored in more depth in a future investigation.

7.1.2. CFD temperature results for MRILEM

The instantaneous results of temperature for the three different temperature conditions are illustrated in Fig. 5, obtained using a combination of the step and β-PDF with c(O_2) and c(h_{298}). These results indicate a subtle variation in the structure of the ignited spray. While the difference is minimal in terms of the progress variable's definition, it becomes clearer, especially for T = 800 K, when comparing the effects of different probability density functions (PDFs). Specifically, the spray has a slightly larger form when employing the β-PDF in contrast to the step PDF. However, differences in other plots are less noticeable. Therefore, further investigation of additional quantities, as discussed in the following sub-sections, is essential for a more comprehensive understanding of differences in progress variable definitions and PDFs.

7.1.3. Apparent heat release rates for MRILEM

Fig. 6 depicts the heat release rate curves for the simulated ECN spray B cases. At T = 800 K, all heat release curves show a strong peak at the start of the simulation around CAD = 1. The reason is the initial 0D reactor solution that does not include turbulence chemistry interactions. It is essential to recall that the solution table for $\dot{c}$ is not initialized from the 0D reactor, which means that any ignition information comes directly from advancing the LEM. In addition, it appears that c(h_{298}) gives a better ignition than c(Y_{O_2}) in the sense that it is closer to experimental results. However, this is only the case for the step-PDF; when analyzing the β-PDF, it appears that the peak for c(h_{298}) is in the same order as c(Y_{O_2}), although ignition delay for c(h_{298}) is always better than c(Y_{O_2}). The remainder of the heat release rate for CAD > 3 shows reasonable results compared to experiments, which indicates that LEM has overwritten the initial 0D reactor initial solutions in the table with values from advancing the LEMs as discussed in the previous paragraph, Fig. 4. Comparing c(h_{298})-Step and c(h_{298})-β shows that in addition to the need for a solution that incorporates turbulence chemistry interaction, the choice of the PDF for integrating in c space has a mayor influence on the solution and can lead to an overestimated heat release curve at T = 900 K

which shows the same trend as the case with T = 800 K, however, less prominent. The reason would be that in case of higher temperatures, the LEM manages to overwrite the solution table more quickly than in lower temperatures, which gives values of similar order to the results predicted by experiments. This is illustrated even more clearly for T = 1000 K, where the initial section of the heat release curve predicts experiments well but with a slight early ignition. Both in T = 900 K and T = 1000 K, the rest of the heat release curve is well predicted, especially the peak value, which shows the satisfactory performance of RILEM. For high-temperature cases, the choice of the PDF has minimal impact on the results. It appears that RILEM solutions are sensitive during the initial stages, particularly in scenarios characterized by low TDC ambient temperatures. This sensitivity may originate from RILEM's inherent limitations to rapidly overwrite the 0D reactor solution with more physically reasonable LEM solutions under such conditions. This point will be investigated in the TRILEM section.

7.1.4. Ignition delay and flame lift-off length for MRILEM

The ignition delay time, denoted as τ_d, is defined following the definition provided by the Engine Combustion Network (ECN) [64]. It suggests that τ_d is equal to the time period from the Start Of Injection (SOI) until the point where the rate of change of the maximum temperature in the domain, represented by dT_{max}/dt, reaches its peak value. The left side of Fig. 7 displays the ignition delay time obtained with MRILEM compared with the experimental value. Ignition delay is better predicted when utilizing the step function PDF combined with c(h_{298}); it is slightly over-predicted at T = 1000 K. Since the entire solution space of species mass fractions is already initialized, the ignition delay time is strictly linked to the development of the reaction progress source term $\dot{c}$, which is provided uniquely by the LEM. Combining the step function and calculating $\dot{c}$ based on c(h_{298}), yields the best results.

The right side of Fig. 7 compares the calculated flame lift-off length with the experimental values. The lift-off length depicted in both figures is also calculated based on the ECN definition [64], which determines it as the shortest distance from the nozzle to the spot where OH mass fraction reaches 14% of its maximum value. The species mas fractions solution table is initialized from the 0D reactor. Similar to the ignition delay times, utilizing the step-PDF combined with c(h_{298}) aligns more closely with experiments. Utilizing the β-PDF causes the selected data to be more intense as it gives more importance to where the mean is located contrary to the step-PDF. Specifically in the scenario where $\tilde{c}$ = 0.5, where uniform importance is attributed to the entire OH mass fraction in c space, as could be observed from comparing Fig. 8 and Fig. 9. This can potentially lead to an elongation of the lift-off length.
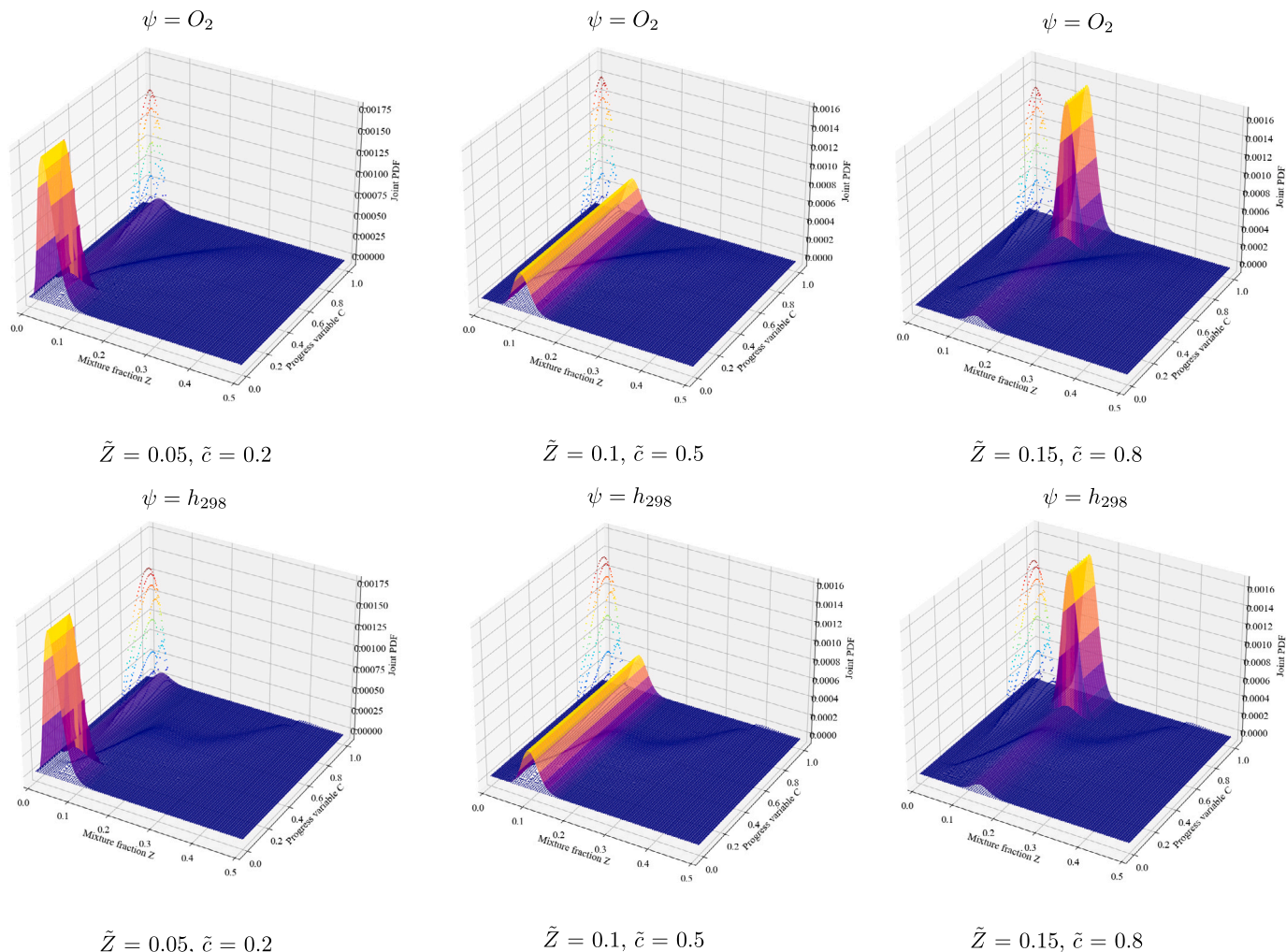
Fig. 8. Representation of the intersection between the Joint PDF of β_Z, step$_c$ and the LEM statistics extracted from $\psi = O_2$ (above) and $\psi = h_{298}$ (below). The β functions were constructed with a $\widetilde{Z''^2} = 0.0004$. The Joint PDF was scaled down to match the size of the OH solution statistics.

7.1.5. Evolution of the reaction progress variable source term

Fig. 10 illustrates the temporal development of $\dot{c}$ for c(Y_{O_2}) and c(h_{298}), employing both the step- and the β-PDF for integration in progress variable space at TDC ambient temperature of $T = 800$ K. It appears that $\dot{c}$ reaches different values for the same Z, c combination in time. This phenomenon is well described when selecting specific bins of Z and c and plotting them in progress variable and mixture fraction space, respectively. When examining the bin $Z = 0.05$, $\dot{c}$, for both c(Y_{O_2}) and c(h_{298}), $\dot{c}$ maintains a high value at $c = 0.2$, it then gets attenuated when reaching later times. A similar pattern is observed for the other element of the figure, i.e., $\dot{c}$ in Z space, in particular for c bin $c = 0.24$, where it reaches high values for $Z \approx 0.1$ for both c(Y_{O_2}) and c(h_{298}) at early phases, and then gets reduced at later stages of the simulation. The reason behind this behavior is the turbulence chemistry interaction on the LEM line, where the turbulence level influences the development of $\dot{c}$ in Z, c space. Furthermore, variations in the $\dot{c}$ distribution across Z and c space are noticeable, due to the choice of progress variable PDF. These discrepancies are attributed to the fact that utilizing different PDFs can alter the combustion process, leading to a different distribution of turbulent scalars on the LEM side, i.e., a change in turbulence chemistry interaction.

This effect can be observed by analyzing Fig. 7 and Fig. 10. In the second row of Fig. 10 at CAD = 2, $\dot{c}$ features inferior values in c space for step and c(h_{298}) at lower regions of c space compared to other configurations. This suggests that utilizing c(h_{298}), combined with a step function, causes the progress of $\tilde{c}$ on the CFD to be slower than in

other configurations, thus a longer ignition delay time as depicted in 10. Additionally, the same plot reveals that for bin $Z = 0.08$, statistics are available for the step function but not for the β-PDF at $c > 0.5$. These observations imply that conditioning the reactive scalars on Z and c for constructing a general solution table may require even the choice of the PDF utilized for integrating into c space. In addition, another turbulence dimension to condition the reactive scalars on, such as turbulence diffusivity D_t or the turbulent Reynolds number Re_t, can further characterize turbulence. This point, however, will be discussed in detail in the next section.

7.2. Tabulated RILEM

TRILEM is essentially a CFD simulation, where no LEM is advanced. The combustion closure in this framework is realized by integrating the turbulent reactive scalars from a pre-constructed solution table using PDFs of Z and c. The solution table utilized in this work is the output of previous MRILEM runs. In this article, TRILEM was applied to the same cases investigated earlier using MRILEM, i.e., the ambient temperatures at TDC of $T = 800$, 900, and 1000 K. The solution tables utilized to advance each TRILEM simulation were extracted from the corresponding MRILEM simulation using the same c PDF. It is important to note that combustion characteristics and heat effects, such as the change in enthalpy caused by the spray are captured through tabulation in both Z and c space. This was possible through the LEM pressure coupling technique developed in [31], where the objective was
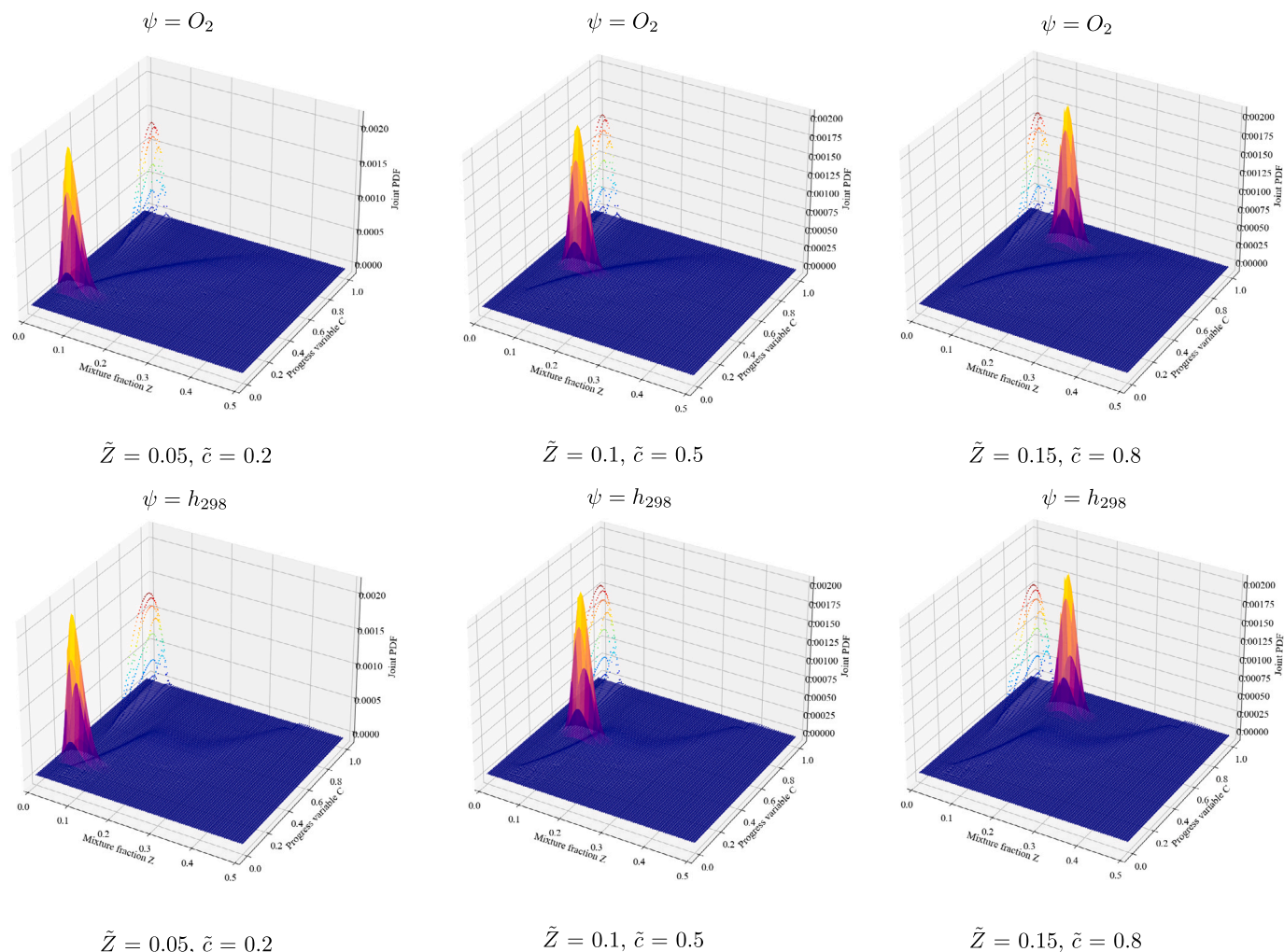
Fig. 9. Representation of the intersection between the Joint PDF of β_Z, β_c and the LEM statistics extracted from $\psi = O_2$ (above) and $\psi = h_{298}$ (below). The β functions were constructed with a $\widetilde{Z''^2} = 0.0004, \widetilde{c''^2} = 0.0004$. The Joint PDF was scaled down to match the size of the OH solution statistics.

to inherently account for the heat effects along the process without relying on external modeling.

7.2.1. Apparent heat release rates for TRILEM

Fig. 11 displays the heat release curves obtained with TRILEM. At $T = 800$ K, the peak of the heat release curves is not as high as in MRILEM. This discrepancy may be attributed to two primary factors. Firstly, the scaling technique applied $\dot{c}$ for MRILEM, since it is not pre-initialized with the homogeneous reactors, unlike the other reactive scalars. However, TRILEM incorporates a solution for all the reactive scalars, including $\dot{c}$, which implies that the scaling effect is substantially reduced in TRILEM compared to MRILEM for $\dot{c}$. Secondly, the discrepancy in TRILEM and MRILEM heat release curves may also be due to the difference between the species mass fraction distribution between LEM and the homogeneous reactors. As depicted in Fig. 4, the LEM solution incorporates effects of molecular diffusion and heat conduction alongside turbulence chemistry interaction, which are not included in the 0D reactor solution. In addition, Fig. 11 also shows that while the choice of utilizing c(Y_{O_2}) or c(h_{298}) does impact the results, the overall effect remains insignificant. At higher TDC ambient temperatures, i.e., $T = 900$ K and $T = 1000$ K, the heat release curves predicted by TRILEM align closely with experiments, except for a discrepancy in the early stages of ignition, which will be discussed in the next paragraph.

7.2.2. Ignition delay and flame lift-off length for TRILEM

The left side of Fig. 12 represents the ignition delay time for TRILEM. As was clarified before, $\dot{c}$ solution is populated in the pre-constructed LEM solution, which means that when integrating $\dot{c}$ on the CFD side with a step- or a β-PDF in c space, high values of $\dot{c}$, that correspond to a burnt state will be taken into consideration depending on the selected PDF of c. This is well illustrated in Fig. 13. When examining the first column of Fig. 13, a comparison between $\psi = O_2$ with step-PDF and $\psi = O_2$ using β-PDF reveals noticeable differences. Specifically, the joint PDF curve, constructed using the step function for $\tilde{Z} = 0.05$ and $\tilde{c} = 0.2$ represented by the blue line, captures larger values of $\dot{c}$ for that Z bin present in high regions of c space than the joint PDF curve constructed using the β function with a $\tilde{c}''^2 = 0.2$, which represents the highest value observed during the simulation, for $\tilde{Z} = 0.05$ and $\tilde{c} = 0.2$ also represented by a blue line. This leads to larger values of $\dot{c}$ on the CFD when employing the step function, which can cause a shorter ignition delay time. This effect is observed in Fig. 12. A similar behavior is also observed when using $\psi = h_{298}$. The TRILEM fast ignition is, however, prominent only for $T = 800$ K. For other temperatures, the ignition delay predicted by TRILEM is in the order of experimental results. This indicates that chemistry becomes the rate-controlling process for high temperatures.

The right side of Fig. 12 depicts the mean lift-off length predicted by TRILEM. TRILEM exhibits improved performance in predicting the mean lift-off lengths compared to MRILEM, which is initialized with 0D reactor solution, especially noticeable at $T = 800$ K. This improvement
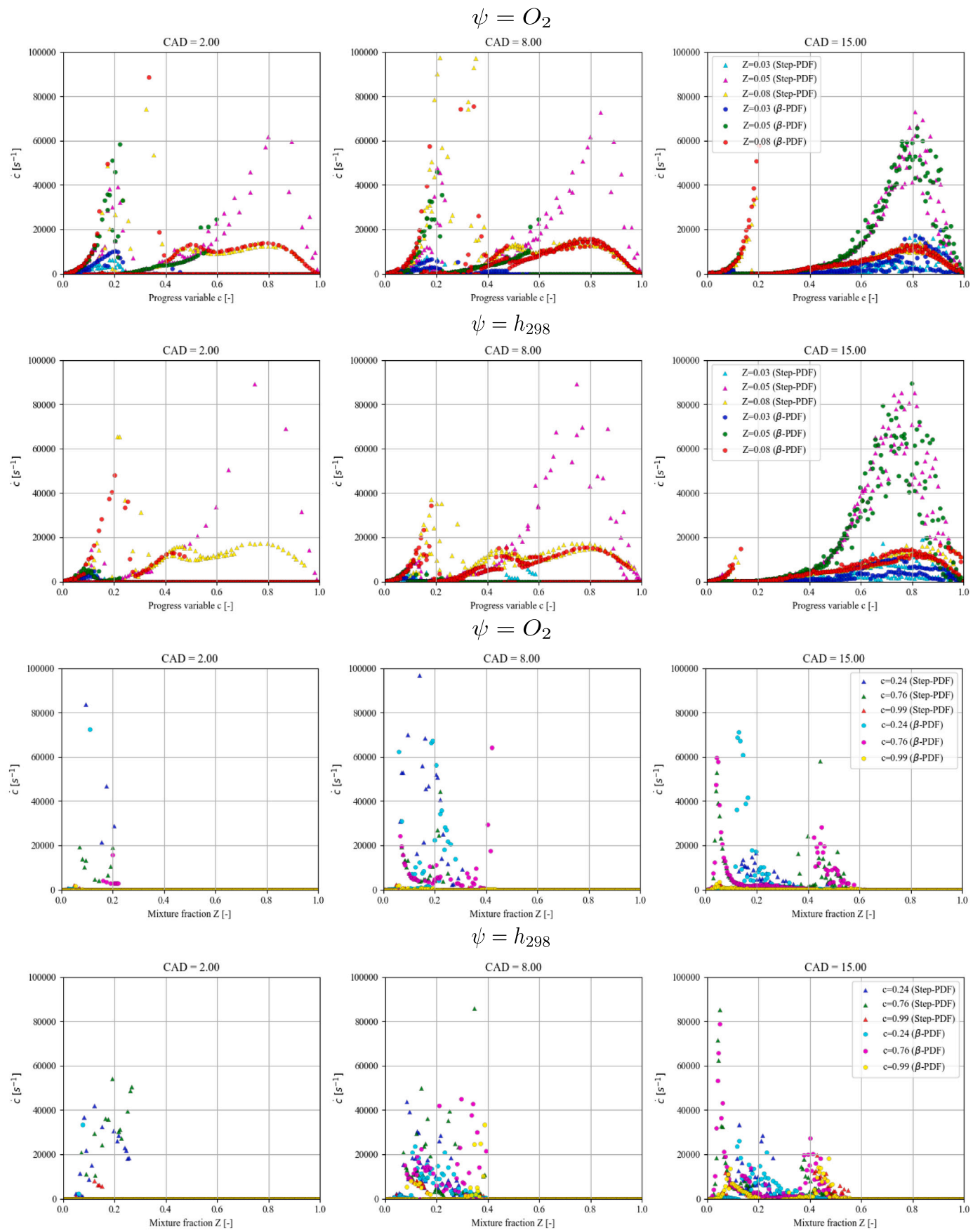
$$\psi = O_2$$

$$\psi = h_{298}$$

$$\psi = O_2$$

$$\psi = h_{298}$$

Fig. 10. Scatter plots of $\dot{c}$ in progress variable space c (above) and mixture fraction Z space (below) for $\psi = O_2$ and $\psi = h_{298}$., and step and β-PDF integration at $T = 800$ K.
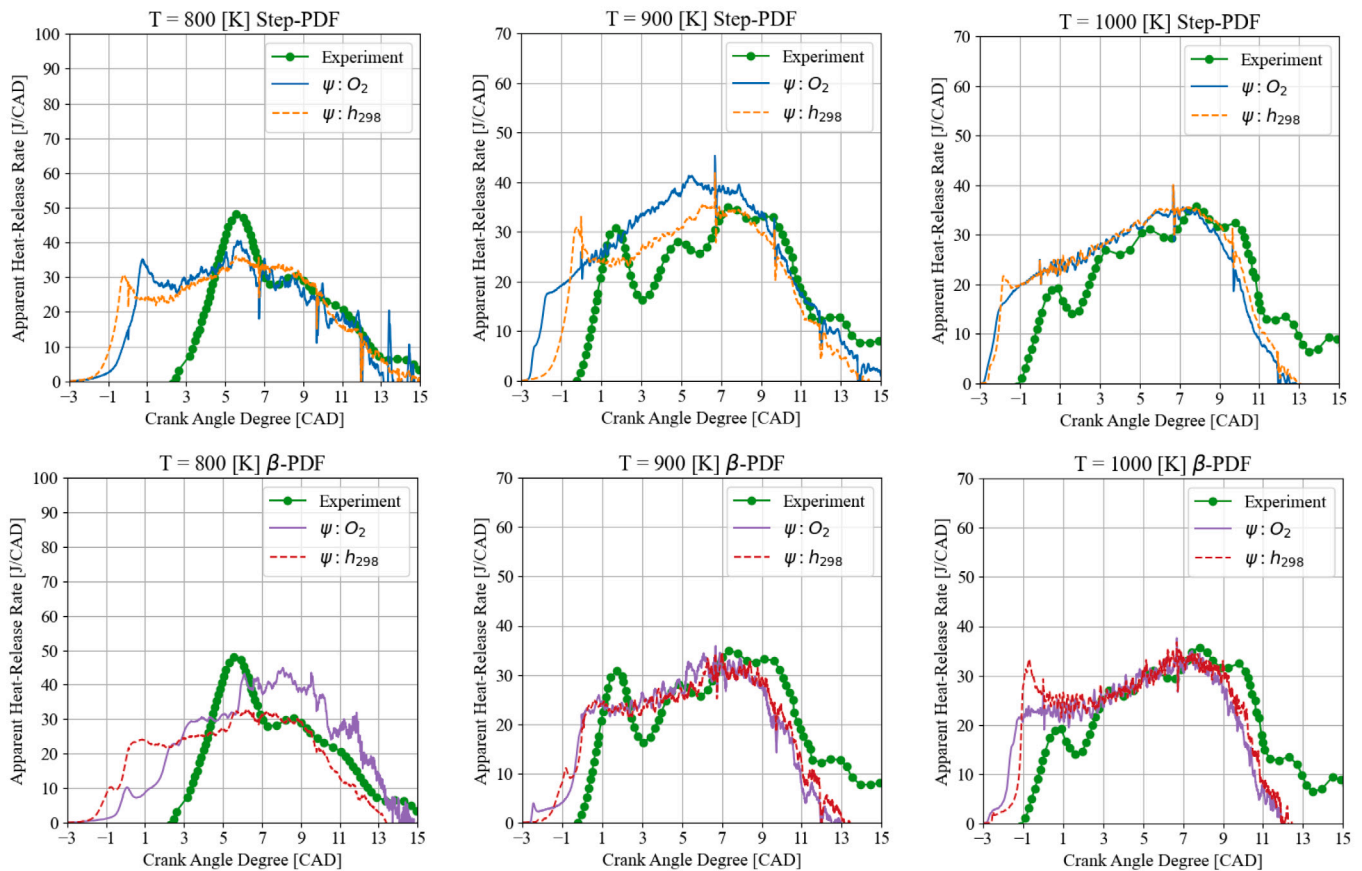
Fig. 11. Comparison of heat release rates for TRILEM for $\psi = O_2$ and $\psi = h_{298}$. and P_c: step (above) and P_c: β (below) with experiments at $T = 800$ K, 900 K and 1000 K.
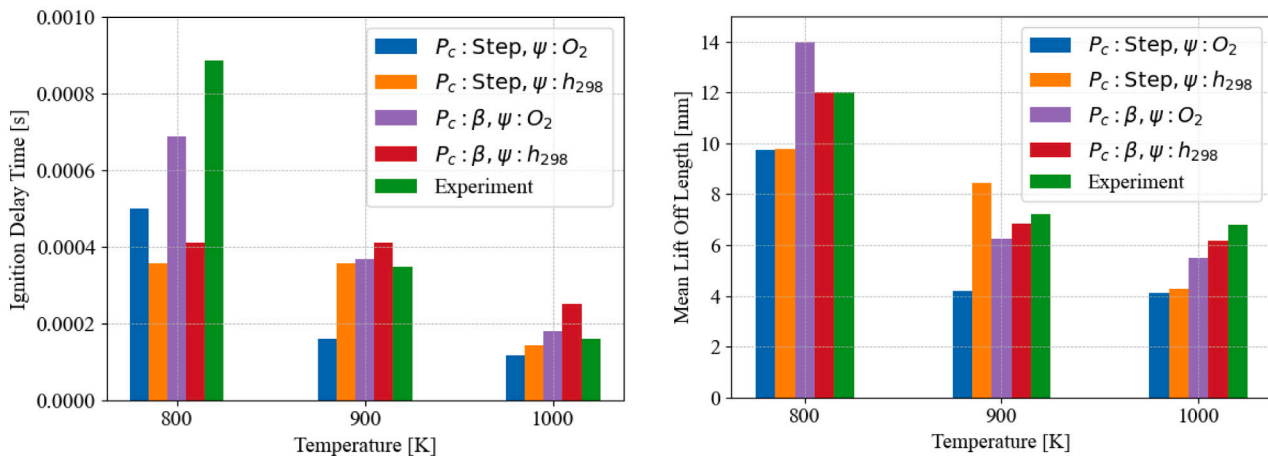

Fig. 12. Comparison of TRILEM ignition delay time (left) and Flame lift-off length (right) with experiments.

is attributed to the development of $\tilde{c}$ on the CFD side, which is governed by the evolution of $\dot{c}$. This effect is illustrated in Fig. 14, which compares the lift-off lengths for both TRILEM and MRILEM for $T = 800$ K, also represented in Fig. 7 and Fig. 12, respectively. The case of $T = 800$ K with $\psi = h_{298}$ combined with β-PDF for c was selected due to its significant improvement in mean lift-off length predictions. As displayed in Fig. 14, the improvement is linked to the development of $\tilde{c} = 0.85$, represented by a red isoline. The choice of this specific $\tilde{c}$ value is due to its representation where OH mass fractions are at their peak in the c space, as depicted in Fig. 4 for both LEM and homogeneous reactors solutions. The development of $\tilde{c}$ in the CFD is governed by

$\dot{c}$. The absence of pre-computed $\dot{c}$ statistics from the homogeneous reactors leads to scaling the PDFs, which results in an overestimation of $\dot{c}$ in regions near the nozzle. This causes an inaccurate development of $\tilde{c}$ in that region. On the other hand, TRILEM employs a pre-constructed solution of $\dot{c}$. Although PDF scaling is also applicable in this case, it is, however, less significant as the majority of the slots in Z, c space are filled in the $\dot{c}$ preconstructed solution. This leads to proper progress of $\tilde{c}$, which ensures an accurate distribution of OH mass fraction, yielding a means lift-off length matching experiments.
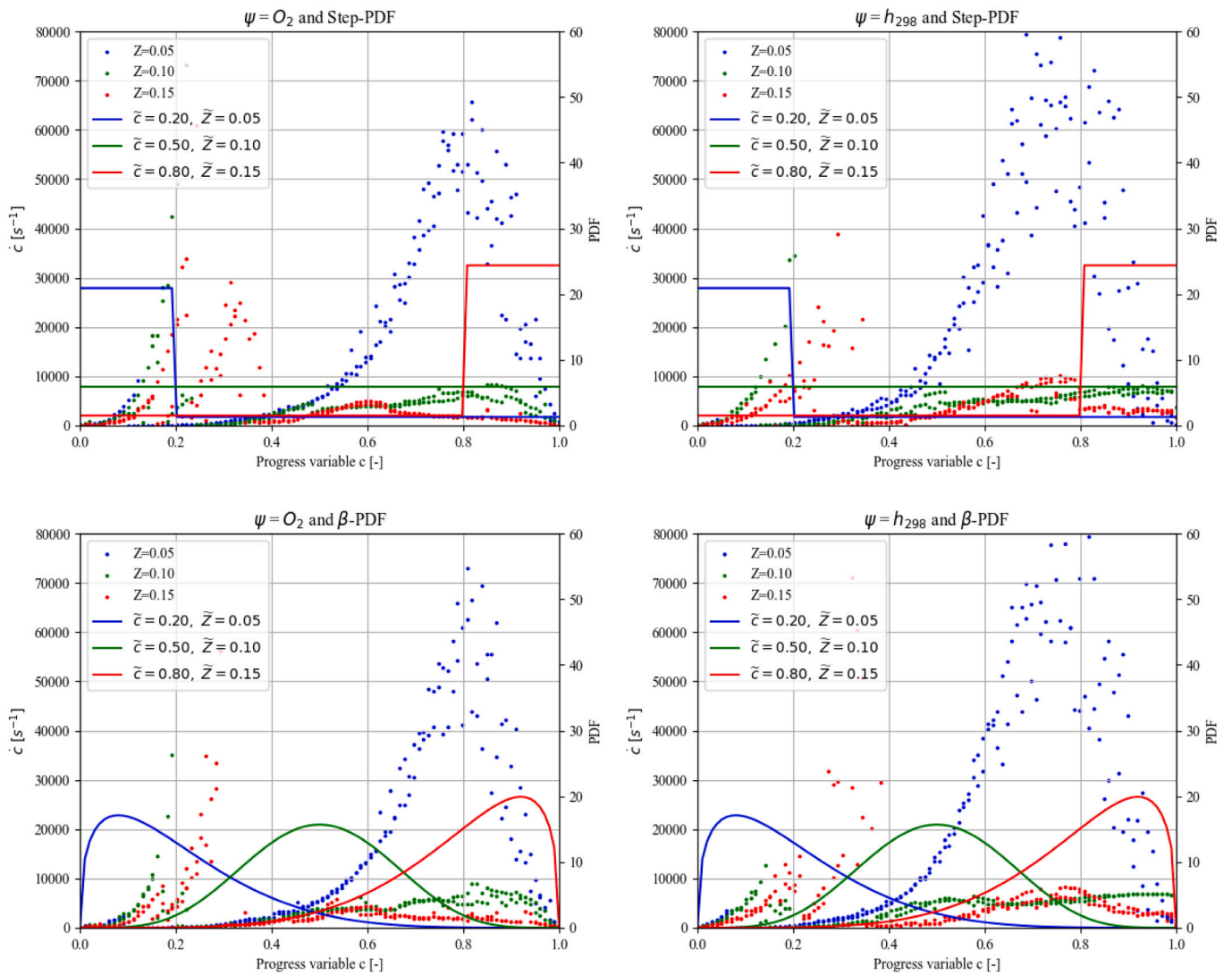
Fig. 13. Representation of the overlap between the statistics of $\dot{c}$ in c space generates based on O_2 (left) or h_{298} (right) and either the step- (above) or the β (below) for PDF of c. The β functions for Z and c were generated a variance of 0.004 and 0.02, respectively. (For interpretation of the references to color in this figure legend, the reader is referred to the web version of this article.)
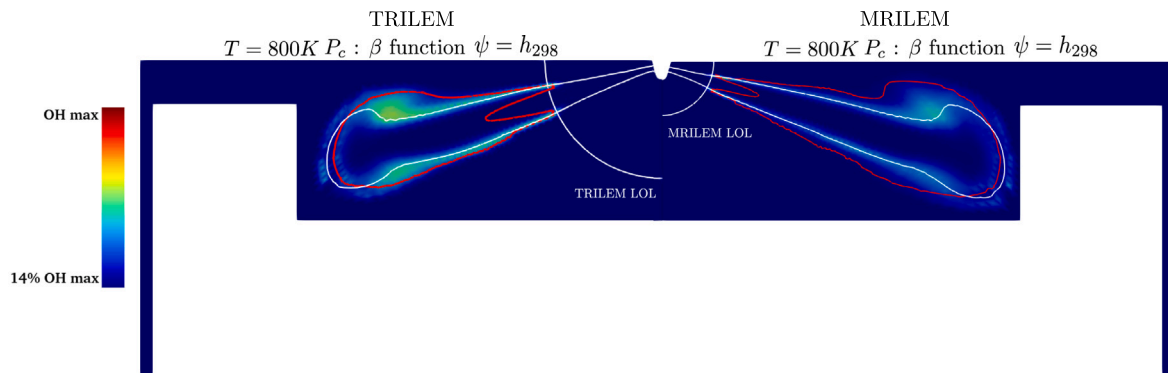

Fig. 14. Comparison of Lift-Off Lengths in TRILEM and MRILEM with $\psi = h_{298}$ and β-PDF for c: Stoichiometric mixture fraction $Z_{st} = 0.045$ (White line) and $\tilde{c} = 0.85$ (Red line). (For interpretation of the references to color in this figure legend, the reader is referred to the web version of this article.)

7.3. Computation time

Fig. 15 displays the computational times for MRILEM and TRILEM, highlighting a significant 4.5 fold improvement in computational time

with TRILEM compared to MRILEM. It also illustrated a minimal difference when using the step and β function in terms of computational time for both models, suggesting that the β function generation is not the bottleneck of the simulation, rather, it is the advancement
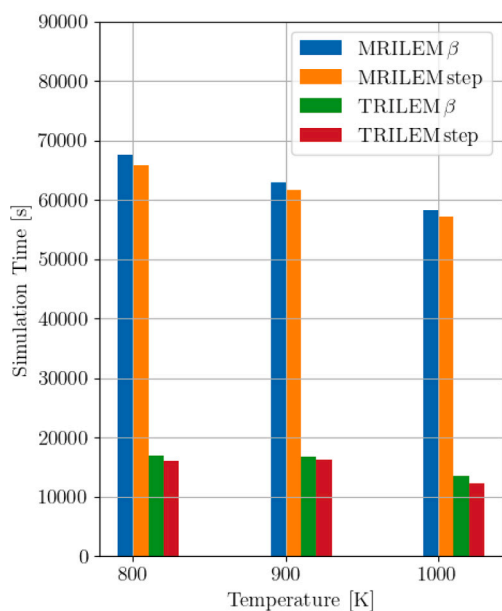
Fig. 15. Simulation times for MRILEM and TRILEM for T=800 K, T=900 K and T=1000 K.

of LEM chemistry. Despite the computational efficiency that TRILEM provides, the gain reported does not correspond to what is delivered by typical tabulation methods. This is because of the turbulence level in this specific case. In high turbulent scenarios, such as duct injection, turbulence on the LEM line would increase, leading to the generation a smaller Kolmogorov length. As LEM resolves all turbulent scales, the LEM line will refine, impling chemistry advancement on more LEM cells, which directly contributes to increasing the computational time. In such a scenario, the TRILEM approach would simulate the case much faster than MRILEM. However, to accurately simulate unsteady effects, the TRILEM table necessitates to be generated using turbulence levels that matched the CFD. The computational gain that the TRIELM can potentially bring for a highly turbulent case was not yet reported, and could be the subject of a future study.

8. Conclusion

In this article, RILEM was tested with two new variants, i.e., Multiple-RILEM with 0D reactor solution initialization and Tabulated-RILEM. These two models were applied for the ECN Sandia-B heavy-duty engine case for three ambient temperatures at TDC. Two definitions of the combustion progress variable were investigated, i.e., $\psi = O_2$ and $\psi = h_{298}$. Moreover, two PDFs for integrating in-progress variable space were assessed, i.e., step and β functions. The fundamental modeling problem of progress variable definition and PDF was not solved in this study. RILEM initialized with the 0D reactor solution demonstrated that utilizing an initial solution that ignores molecular diffusion, heat conductivity, and turbulence chemistry interaction leads to a sudden ignition, releasing extensive heat compared to experiments. The heat release results reach normal levels at later simulation stages when the LEM overwrites the initial solutions. Utilizing $\psi = h_{298}$ showed to give better results overall compared to $\psi = O_2$. In addition, utilizing the step function produced better results than the β PDF. However, the variance of the combustion progress variable was derived based on a newly developed RANS adaptation of the Pierce and Moin formulation [57], which was originally suggested for LES. Additionally, the model's relative performance may be case-dependent and clarification is left for future studies. In the case of TRILEM, no big difference was spotted when utilizing $c(Y_{O_2})$ and $c(h_{298})$ or step and β PDF, for

that it is suggested to stick with the step PDF since it requires less time. This is valid only for predictions of heat release rate. However, when utilizing β, TRILEM performs better than MRILEM for predicting ignition delay times and lift-off lengths. It has been detected in this work that there is a dependency of $\dot{c}$ on time. The change of $\dot{c}$ was due to turbulence and diffusion and conduction that changes across the period of the LEM realization. This means that utilizing either MRILEM or TRILEM with an initialization of $\dot{c}$ may not yield the most accurate results. Instead, an additional dimension considering the turbulence level is required in addition to Z and c. A computational gain of 4.5 folds was also reported when utilizing TRILEM over MRILEM. However, the gain could be much more significant in an case that features higher turbulence levels.

CRediT authorship contribution statement

Nidal Doubiani: Writing – review & editing, Writing – original draft, Visualization, Validation, Software, Methodology, Investigation, Formal analysis, Data curation. **Michael Oevermann:** Writing – review & editing, Supervision, Project administration, Methodology, Investigation, Funding acquisition, Formal analysis.

Declaration of competing interest

The authors declare that they have no known competing financial interests or personal relationships that could have appeared to influence the work reported in this paper.

Data availability

Data will be made available on request.

References

[1] International Energy Agency. Cars and vans - energy system. 2023.

[2] Reitz Rolf D, et al. IJER editorial: The future of the internal combustion engine. Int J Engine Res 2020;21(1):3–10.

[3] Boningari Thirupathi, Smirniotis Panagiotis G. Impact of nitrogen oxides on the environment and human health: Mn-based materials for the NOx abatement. Curr Opin Chem Eng 2016;13:133–41.

[4] Kao Louise W, Nanagas Kristine A. Toxicity associated with carbon monoxide. Clin Lab Med 2006;26(1):99–125.

[5] Joshi Ameya. Review of vehicle engine efficiency and emissions. SAE Int J Adv Curr Pract Mobil 2020;2(2020-01-0352):2479–507.

[6] Requia Weeberb J, et al. How clean are electric vehicles? Evidence-based review of the effects of electric mobility on air pollutants, greenhouse gas emissions and human health. Atmos Environ 2018;185:64–77.

[7] Liu Xinyu, et al. Comparison of well-to-wheels energy use and emissions of a hydrogen fuel cell electric vehicle relative to a conventional gasoline-powered internal combustion engine vehicle. Int J Hydrog Energy 2020;45(1):972–83.

[8] Sinay Juraj, et al. Analysis of the risks of hydrogen leakage from hydrogen-powered cars and their possible impact on automotive market share increase. Appl Sci 2020;10(12):4292.

[9] Bilous Olegh, Amundson Neal R. Chemical reactor stability and sensitivity. AIChE J 1955;1(4):513–21.

[10] Zembi Jacopo, Mariani Francesco, Battistoni Michele. Large Eddy Simulation of Ignition and Combustion Stability in a Lean SI Optical Access Engine. Tech. rep., SAE Technical Paper; 2019.

[11] Silva Mickael, et al. Effects of Geometry on Passive Pre-Chamber Combustion Characteristics. Tech. rep., SAE Technical Paper; 2020.

[12] Vulis Lev Abramovich, Friedman Morris D, Williams Glenn C. Thermal regimes of combustion. 1961.

[13] Lu Hao, et al. Large-eddy simulation of sandia flame f using structural subgrid-scale models and partially-stirred-reactor approach. Phys Fluids 2019;31(4).

[14] Qian Xiang, et al. Large-eddy simulation of cambridge-sandia stratified flames under high swirl. Combust Flame 2022;244:112241.

[15] Pitsch Heinz, Chen M, Peters Norbert. Unsteady flamelet modeling of turbulent hydrogen-air diffusion flames. In: Symposium (international) on combustion, vol. 27, (1):Elsevier; 1998, p. 1057–64.

[16] Benajes Jesus, et al. Unsteady flamelet modeling study on OMEx-type fuels under engine combustion network spray A conditions. Fuel 2023;331:125458.

[17] Peters Norbert. Turbulent combustion. Cambridge University Press; 2000.

[18] Nilsson P, Bai Xue-Song. Level-set flamelet library approach for premixed turbulent combustion. Exp Therm Fluid Sci 2000;21(1–3):87–98.

[19] Maghbouli Amin, et al. Modelling compression ignition engines by incorporation of the flamelet generated manifolds combustion closure. Combust Theory Model 2019;23(3):414–38.

[20] Almutairi FS, Dinesh KKJ Ranga, van Oijen JA. Modelling of hydrogen-blended dual-fuel combustion using flamelet-generated manifold and preferential diffusion effects. Int J Hydrog Energy 2023;48(4):1602–24.

[21] Klimenko Alex Y, Bilger Robert William. Conditional moment closure for turbulent combustion. Prog Energy Combust Sci 1999;25(6):595–687.

[22] Sekularac Nikola, et al. Conditional space evaluation of progress variable definitions for cambridge/sandia swirl flames. Combust Theory Model 2023;1–32.

[23] Zhang YZ, Kung EH, Haworth DC. A PDF method for multidimensional modeling of HCCI engine combustion: effects of turbulence/chemistry interactions on ignition timing and emissions. Proc Combust Inst 2005;30(2):2763–71.

[24] Kung EH, Haworth DC. PDF methods in real engine geometries. In: 5th US combustion meeting 2007. Combustion Institute; 2007, p. 2354–60.

[25] Kerstein Alan R. A linear- eddy model of turbulent scalar transport and mixing. Combust Sci Technol 1988;60(4–6):391–421. http://dx.doi.org/10.1080/00102208808923995.

[26] Kerstein Alan R. Linear-eddy modelling of turbulent transport. Part 3. Mixing and differential molecular diffusion in round jets. J Fluid Mech 1990;216:411–35. http://dx.doi.org/10.1017/S0022112090000489, Publisher: Cambridge University Press.

[27] Kerstein Alan R. Linear-eddy modelling of turbulent transport. Part 6. Microstructure of diffusive scalar mixing fields. J Fluid Mech 1991;231:361–94. http://dx.doi.org/10.1017/S0022112091003439.

[28] McMurtry PA, Menon S, Kerstein AR. Linear eddy modeling of turbulent combustion. Energy Fuels 1993;7(6):817–26.

[29] Cremer MA, McMurtry PA, Kerstein AR. Effects of turbulence length-scale distribution on scalar mixing in homogeneous turbulent flow. Phys Fluids 1994;6(6):2143–53.

[30] Chakravarthy VK, Menon S. Linear eddy simulations of Reynolds number and Schmidt number effects on turbulent scalar mixing. Phys Fluids 2001;13(2):488–99.

[31] Doubiani Nidal, et al. Pressure coupling of the spherical linear eddy model to RANS-cfdfor internal-combustion engine simulation. 2021, http://dx.doi.org/10.11159/csp21.lx.103.

[32] Menon Suresh, Calhoon, Jr. William H. Subgrid mixing and molecular transport modeling in a reacting shear layer. In: Symposium (international) on combustion, vol. 26, (1):Elsevier; 1996, p. 59–66.

[33] Gonzalez Esteban, et al. Turbulent-combustion closure for the chemical source terms using the linear-eddy model. In: 53rd AIAA/SAE/ASEE joint propulsion conference. 2017, p. 5080.

[34] Gonzalez Esteban, et al. Effect of the turbulence modeling in large-eddy simulations of nonpremixed flames undergoing extinction and reignition. In: 55th AIAA aerospace sciences meeting. 2017, p. 0604.

[35] Arshad Salman, et al. A strategy for large-scale scalar advection in large eddy simulations that use the linear eddy sub-grid mixing model. Internat J Numer Methods Heat Fluid Flow 2018;28(10):2463–79. http://dx.doi.org/10.1108/HFF-09-2017-0387.

[36] Arshad Salman, et al. Subgrid reaction-diffusion closure for large eddy simulations using the linear-eddy model. 2019, p. 28.

[37] El-Asrag Hossam, Menon Suresh. Large eddy simulation of a swirling non-premixed flame. In: 41st AIAA/aSME/SAE/ASEE joint propulsion conference & exhibit. 2005, p. 3971.

[38] Sankaran V, Menon S. Subgrid combustion modeling of 3-D premixed flames in the thin-reaction-zone regime. Proc Combust Inst 2005;30(1):575–82.

[39] Li Shaoshuai, et al. A large-eddy simulation–linear-eddy model study of preferential diffusion processes in a partially premixed swirling combustor with synthesis gases. J Eng Gas Turbines Power 2017;139(3).

[40] Menon Abhilash Murlidharan. Super-grid linear eddy model (SG-LEM): Efficient mode-and regime-independent combustion closure for large eddy simulation (LES). Chalmers Tekniska Hogskola (Sweden); 2022.

[41] Menon Abhilash M, Oevermann Michael, Kerstein Alan R. A super-grid approach for LES combustion closure using the linear eddy model. Combust Theory Model 2023;1–28.

[42] Goldin Graham, Menon Suresh, Calhoon William H Jr. A linear eddy mixing model for steady non-premixed turbulent combustion. In: 33rd aerospace sciences meeting and exhibit. 1995, p. 379.

[43] Sannan Sigurd, Weydahl Torleif, Kerstein Alan R. Stochastic simulation of scalar mixing capturing unsteadiness and small-scale structure based on mean-flow properties. Flow Turbul Combust 2013;90:189–216.

[44] Lackmann Tim, Kerstein Alan, Oevermann Michael. A representative interactive linear eddy model (RILEM) for non-premixed combustion. 2015, http://dx.doi.org/10.4271/2015-01-0390, 2015–01–0390.

[45] Lackmann Tim, Kerstein Alan R, Oevermann Michael. Comparison of a representative linear eddy model with a representative interactive flamelet model for spray combustion processes. 2015, p. 2015–4–2466. http://dx.doi.org/10.4271/2015-24-2466.

[46] Lackmann Tim, et al. Investigation of turbulence–chemistry interactions in a heavy-duty diesel engine with a representative interactive linear eddy model. Int J Engine Res 2020;21(8):1469–79. http://dx.doi.org/10.1177/1468087418812319, Publisher: SAGE Publications.

[47] Doubiani Nidal, Kerstein Alan R, Oevermann Michael. A pressure-coupled representative interactive linear eddy model (RILEM) for engine simulations. Fuel 2024;355:129423.

[48] Kerstein Alan R. Linear-eddy modeling of turbulent transport. Part 4. Structure of diffusion flames. Combust Sci Technol 1992;81(1–3):75–96. http://dx.doi.org/10.1080/00102209208951794.

[49] Kerstein Alan R. Linear-eddy modelling of turbulent transport. Part 7. Finite-rate chemistry and multi-stream mixing. J Fluid Mech 1992;240:289–313. http://dx.doi.org/10.1017/S0022112092000107, Publisher: Cambridge University Press.

[50] Hindmarsh Alan C, et al. SUNDIALS: Suite of nonlinear and differential/algebraic equation solvers. ACM Trans Math Softw 2005;31(3):363–96.

[51] Goodwin David G, Moffat Harry K, Speth Raymond L. Cantera: An object-oriented software toolkit for chemical kinetics, thermodynamics, and transport processes. 2018.

[52] Lackmann Tim, Kerstein Alan R, Oevermann Michael. A representative linear eddy model for simulating spray combustion in engines (RILEM). Combust Flame 2018;193:1–15. http://dx.doi.org/10.1016/j.combustflame.2018.02.008.

[53] Lackmann Tim, et al. Modeling n-dodecane spray combustion with a representative interactive linear eddy model. 2017-March, (March). 2017, http://dx.doi.org/10.4271/2017-01-0571, SAE Technical Papers.

[54] Lignell David O, et al. One-dimensional turbulence modeling for cylindrical and spherical flows: model formulation and application. Theor Comput Fluid Dyn 2018;32(4):495–520. http://dx.doi.org/10.1007/s00162-018-0465-1.

[55] Gao Zhenxun, Jiang Chongwen, Lee Chun-Hian. Representative interactive flamelet model and flamelet/progress variable model for supersonic combustion flows. Proc Combust Inst 2017;36(2):2937–46. http://dx.doi.org/10.1016/j.proci.2016.06.184.

[56] Bilger RW. The structure of diffusion flames. Combust Sci Technol 1976;13(1–6):155–70.

[57] Pierce Charles D, Moin Parviz. Progress-variable approach for large-eddy simulation of non-premixed turbulent combustion. J Fluid Mech 2004;504:73–97. http://dx.doi.org/10.1017/S0022112004008213.

[58] Eagle W Ethan, Malbec Louis-Marie, Musculus Mark PB. Measurements of liquid length, vapor penetration, ignition delay, and flame lift-off length for the engine combustion network 'Spray B'in a 2.34 L heavy-duty optical diesel engine. SAE Int J Engines 2016;9(2):910–31.

[59] Yao Tong, et al. A hybrid mechanism for n-dodecane combustion with optimized low-temperature chemistry. 2015.

[60] Weller HG, et al. A tensorial approach to computational continuum mechanics using object-oriented techniques. Comput Phys 1998;12(6):620–31. http://dx.doi.org/10.1063/1.168744, Publisher: American Institute of Physics.

[61] Lucchini Tommaso, et al. Automatic mesh generation for CFD simulations of direct-injection engines. English. SAE Technical Paper 2015-01-0376, Warrendale, PA: SAE International; 2015, http://dx.doi.org/10.4271/2015-01-0376.

[62] Bhattacharjee Subhasish, Haworth Daniel C. Simulations of transient n-heptane and n-dodecane spray flames under engine-relevant conditions using a transported PDF method. Combust Flame 2013;160(10):2083–102.

[63] Ranz WE, Marshall WRM. Evaporation from drops, Parts I & II. Chem Eng Prog 1952;48:141–6.

[64] Hawkes ER. Engine combustion network workshop. 2015, Workshop presented in 2015.